A Hybrid-Switching Based Bridgeless PFC Converter for On-Board Battery Chargers using Predictive Current Control

Mohammad Reza Abedi*‡, Brian Ernzen*

*Department of Electrical and Computer Engineering, Baylor University, Waco, TX

mohammadreza_abedi@baylor.edu, brian_ernzen@baylor.edu

‡Corresponding Author; Mohammad Reza Abedi, Department of Electrical and Computer Engineering, Baylor University, Waco, TX,+1 254 548 1566, mohammadreza_abedi@baylor.edu

Received: 02.09.2012 Accepted: 01.10.2012

Abstract- This paper presents a hybrid-switching based bridgeless PFC converter for on-board battery chargers. Using this novel topologythe front-end full-bridge rectifierhas beeneliminated resulting in performance, size, and cost advantage over conventional bridge type PFC converters.Unity power factor and very low total harmonic distortion (THD) is achieved over wide input voltage and load current range using Predictive Current Control (PCC) for hybrid-switching based bridgeless PFC converter. The control law is derived for an accurate model of the converter including parasitic elements. To investigate the dynamic performance of the PFC rectifier, the small-signal models are derived. Input voltage feed-forward compensation provides sinusoidal input current and a desired output voltage even if the input voltage is disturbed. Simulation results show the effectiveness of using predictive current control for hybrid-switching based bridgeless PFC converter.

Keywords- Hybrid-Switching Based Bridgeless PFC Converter, On-Board Battery Charger, Predictive Current Control (PCC)

1. Introduction

Recently, some of major cities in the world formulates a policy and encourages popularizing an eco-friendly vehicle, typically Electric Vehicles (EVs) and Plug-In Hybrid EVs (PHEVs). In order to speed up its commercial launching in the market, it is necessary to obtain a high-efficiency battery and its charger technology, which is the key power source of the vehicles. Among of various batteries, Nickel Metal Hydride (Ni-MH), Lithium-Ion (Li-Ion) and Li-Polymer batteries are mostly being used to have better energy density, efficiency, safety and cost, and the batteries performances are improving. There are two types of chargers for EV application. One is a standalone type which can be compared to a petrol station aimed at fast charge. The other is an on-board type which would be appropriate for slow charge from a house utility outlet during nighttime, when demand of electricity is low. Slow charge overnight is very beneficial for an electricity distribution system [1-2].

Particularly, an on-board battery charger has to be small and light in order to maximize energy efficiency and the distance covered per charging [3]. Therefore, a high frequency switching technique is required to reduce size of passive components, and to minimize switching losses caused by the high frequency switching. The battery charging algorithm point of view, various researches are performed to have better battery charging algorithm, for instance, Constant Voltage (CV), Constant Current (CC), CC-CV, power control and pulse injection method and so on, considering lifecycle, safety and efficiency of the batteries [4-5].

The main part of On-board battery chargers is diode-bridge rectifier followed by PFC circuit in order to improve power factor of input current and output voltage regulation. Low power factor and harmonics have a negative effect on power quality degrading overall system efficiency in power systems. To overcome these deficiencies, AC/DC circuits with active power factor correction (PFC) have been developed [6-7]. These PFC circuits use a bridge followed

by a switch mode circuit that is controlled to actively shape the input current from the AC power source. The most common switch mode circuit used in this application is the boost converter. While being an improvement over the simple bridge rectifier with an output capacitor, these PFC circuits still have a limitation due to high conduction losses in the diodes of the bridge. These conduction losses are especiallyprominent during low input voltage situations in which the input current is large.

Until recently, despite efforts to develop a new circuit that could achieve active PFC without the bridge, it had been assumed that the bridge rectifier in PFC circuits was an unavoidable necessity. However, this is not the case as a new class of converters capable of the direct ac-dc conversion with PFC using hybrid-switching is indeed possible as introduced for the first time in [8].

The overall objective of this paper is the implementation and control of hybrid-switching based PFC converter to provide the high efficient on-board battery chargers. The required small signal analysis for both the positive and negative half cycle of the input line voltage independently. This small signal analysis is required in order to achieve control and perform stability analysis of the bridgeless PFC converter with hybrid switching. Section II proposes the power stage structure of EV on-board battery charger with hybrid-switching based PFC converter. Section III reviews the operation and steady state relations of the bridgeless converter with hybrid switching. Section IV provides the predictive current control of this novel topology for on-board battery chargers. Simulation results demonstrate the validity of this approach in section V.

2. The Power Stage Structure of EV On-Board Battery Charger

The common schematic block diagram of on-board battery charger is depicted in Fig. 1. To prevent conducted harmonics and noise from entering the power supply an input filter has been included in this configuration. The diode-bridge rectifier followed by PFC circuit in order to improve power factor of input current and output voltage regulation is the nature of this typical configuration. The output of EV battery charger needs to be isolated from the main for safety consideration. For dc-dc stage many topologies such as soft-switched full bridge, ZVS half bridge, and soft-switched forward converter can be considered [1-4], which is not our objective in this work.

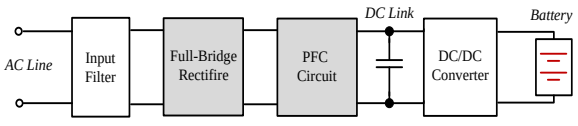

Fig. 1. The overall block diagram of conventional on-board battery charger.

In order to configure the small, light and high efficiency on-board battery charger, the new hybrid switching based bridgeless rectifier followed by dc-dc converter is adopted in this research which is shown in Fig. 2. The bridgeless PFC converter based on novel hybrid switching method (Presented in [8] by Slobodan Cuk) is considered in this configuration to eliminate the front-end full-bridge rectifier resulting in performance, size, and cost advantage over conventional bridge type PFC converters. The novel hybrid switching method enables new Single-Stage ac-dc converter topology, consisting of just three switches and a single magnetic component, to reach a much higher efficiency, higher power factor, and lower total harmonic distortion.

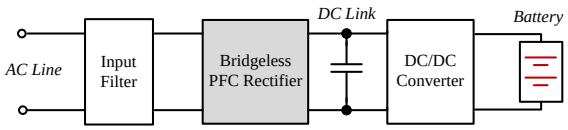

Fig. 2. The overall block diagram of on-board battery charger using the novel hybrid-switching based bridgeless PFC converter.

The novel bridgeless PFC converter requires only a single resonant capacitor and no input inductor compared to the isolated bridgeless converter. Despite the use of a resonant inductor and a resonant capacitor, thanks to the novel hybrid-switching method, the DC voltage gain depends on the duty ratio only and not on resonant component values or the load current.

3. Novel Hybrid Switching Method

3.1. Topology Description

In this bridgeless converter with hybrid switching [8], all full bridge rectifier elements have been eliminated such that this converter operates directly from AC line. As shown in Fig.3, this topology uses three switches: one active switch and two diodes. The active switch controls both diode switches to operate in the correct way for both the positive and negative half cycle of input AC line voltage.

To meet this objective, hybrid switching is utilized, which is the combination of square-wave PWM switching and resonant switching techniques. Hybrid switching operates in a totally different way than conventional resonant and quasi resonant converters. As shown in Fig. 3, this topology consists of a series LC resonant network which has the essential role of utilizing the hybrid-switching in this converter [8].

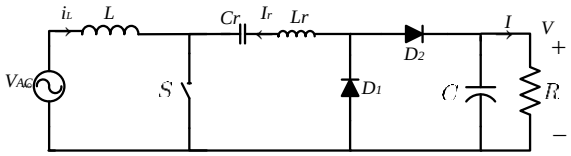

Fig. 3. The novel hybrid-switching based bridgeless PFC converter.

3.2. Steady State Operation

Since the converter includes different electrical configurations for operating in positive and negative half

cycle of the input AC line voltage, operating sequences of the converter should be analyzed for each polarity separately.

The operating subintervals of the converter for the positive half cycle of input AC line are illustrated in Fig. 4. The stateof the active switch S controls which subinterval the converter is in.

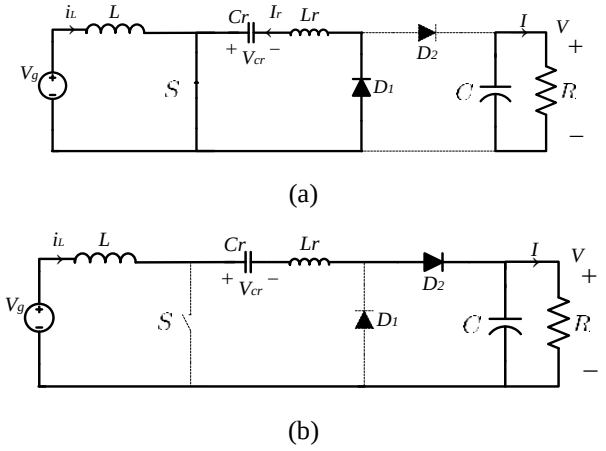

Fig. 4. The operating sequences of the converter for positive half cycle of input AC line a) when the switch is in on state b) when the switch is in off state.

As shown in Fig. 4, during the on-time subinterval of switch S, passive switch D1 conducts and the passive switch D2 does not conduct. During the off-time subinterval of switch S, passive switch D2 conducts in response to the state of S and the passive switch D1 does not conduct.

We assumed that the inductor L is large enough to result in a constant input dc current with ignoring the ac ripple current. During the on-time subinterval of switch S, the following equations can be written

$$L\frac{di(t)}{dt} = v_g(t) \tag{1.a}$$

$$C\frac{dv(t)}{dt} = -\frac{v(t)}{R} \tag{1.b}$$

Where the Eqs. (1.a) and (1.b) are representing the large low-pass filter elements of the converter (L and C), they are designed such that their ripple components are small. During the off-time subinterval of switch S, the following equations can be written

$$L\frac{di(t)}{dt} = v_g(t) - v(t) - v_{Cr}(t) \tag{2.a}$$

$$C\frac{dv(t)}{dt} = i_L(t) - \frac{v(t)}{R} \tag{2.b}$$

As can be seen in Fig.4 the resonant inductor Lr is in series with PWM inductor during the off-time, so resonant inductor current cannot be considered to be a state. Despite the PWM inductor which is flux balanced over the entire switching period, the resonant inductor is excited with a co-sinusoidal ac ripple voltage Δvr of the resonant capacitor Cras shown in Fig. 5 and is fully flux balanced during the on-time interval only.Thus this inductor cannot support any net DC voltage and it circulating energy in the switch S and diode D1. From the resonant circuit in Fig. 4a, we have

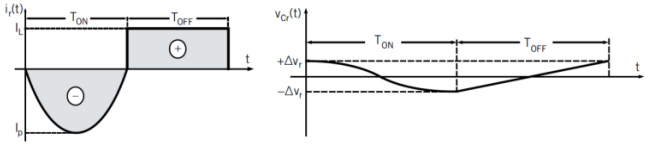

(a) (b)

Fig. 5. Resonant inductor current (a) and resonant capacitor voltage (b) waveforms in one switching cycle during the positive half cycle of input AC line. [8]

$$L_r\frac{di_r(t)}{dt} = v_{Cr}(t) \tag{3}$$

The nonlinear averaged equation for bridgeless converter working in positive half cycle can be extracted from Eqs. (1) and (2) as following

$$L\frac{d\langle i(t)\rangle_{Ts}}{dt} = \langle v_g(t)\rangle_{Ts} - d'(t)\langle v(t)\rangle_{Ts} - d'(t)\langle v_{Cr}(t)\rangle_{Ts} \tag{4.a}$$

$$C\frac{d\langle v(t)\rangle_{Ts}}{dt} = d'(t)\langle i_L(t)\rangle_{Ts} - \frac{\langle v(t)\rangle_{Ts}}{R} \tag{4.b}$$

As mentioned before the resonant inductor is flux balanced during the on-time interval only, this means:

This reduces the Eq. (4) to

$$L\frac{d\langle i(t)\rangle_{Ts}}{dt} = \langle v_g(t)\rangle_{Ts} - d'(t)\langle v(t)\rangle_{Ts} \tag{5.a}$$

$$C\frac{d\langle v(t)\rangle_{Ts}}{dt} = d'(t)\langle i_L(t)\rangle_{Ts} - \frac{\langle v(t)\rangle_{Ts}}{R} \tag{5.b}$$

Eq.(5) is identical to nonlinear equation of Boost converter which was predictable from Fig. 4. As it shown in this figures the circuit is actually operates like a boost converter when the input is positive. The resonant tank has no important role in energy transfer, as it is in series with the current source L, and circulating energy in the switch S and diode D1 .We need these additional resonant switch elements (Lr and Cr), to make the hybrid-switching method possible.

The operating subintervals of the converter for the negative half cycle of the input AC line are illustrated in Fig. 6. Just as in the case of the positive half cycle, the state of the active switch S controls which subinterval the converter is in.As shown in Fig. 6, during the on-time subinterval of switch S, passive switch D2 conducts and the passive switch D1 does not conduct. During the off-time subinterval of switch S, passive switch D1 conducts in response to the state of S and the passive switch D2 does not conduct.Ignoring the ac ripple current with assuming that the inductor L is large enough to result in a constant input dc current. During the on-time subinterval of switch S, the following equations can be written

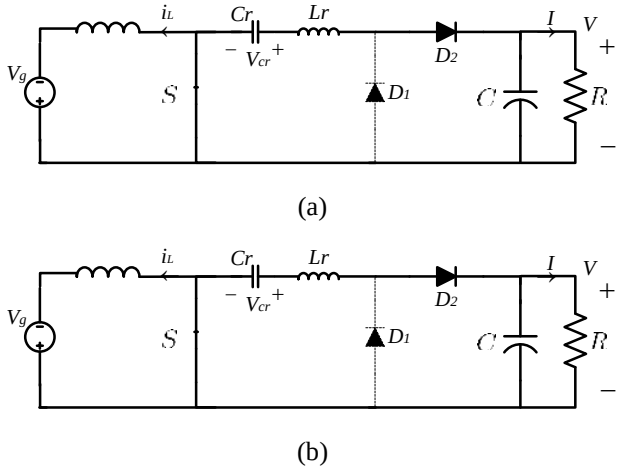

(a)

(b)

Fig. 6. The operating sequences of the converter for negative half cycle of input AC line a) when the switch is in on state b) when the switch is in off state.

$$L\frac{di(t)}{dt} = v_g(t) \tag{6.a}$$

$$C\frac{dv(t)}{dt} = i_{Lr}(t) - \frac{v(t)}{R} \tag{6.b}$$

During the off-time subinterval of switch S, the following equations can be written

$$L\frac{di(t)}{dt} = v_g(t) - v_{Cr}(t) \tag{7.a}$$

$$C\frac{dv(t)}{dt} = -\frac{v(t)}{R} \tag{7.b}$$

Like the positive half cycle of input AC line during the off-time subinterval the resonant inductor Lr is in series with PWM inductor, so the resonant inductor current cannot be considered as a state. Again despite the PWM inductor which is flux balanced over the entire switching period, as shown in Fig. 7 the resonant inductor is fully flux balanced during the on-time interval only.

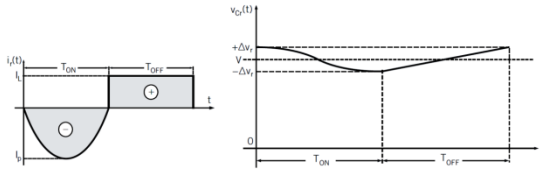

(a) (b)

Fig. 7. Resonant inductor current (a) and resonant capacitor voltage (b) waveforms in one switching cycle during the negative half cycle of input AC line.[8]

In the negative half cycle of line voltage, the operation is quite different from what we had in the positive half cycle. To some extent, it looks like a Cuk converter. The key element is transferring the energy through the resonant capacitor Cr. It receives energy from the inductor L during off-time interval and delivers energy to the load during the on-time interval. The resonant inductor Lr is just used for discharging Cr, keeping the charge balance of the capacitor Cr. From the resonant circuit in Fig. 6a, we have

$$L_r\frac{di_r(t)}{dt} = v_{Cr}(t) - v(t) \tag{8}$$

The nonlinear averaged equation for bridgeless converter working in positive half cycle can be extracted from Eqs. (6) and (7) as following

$$L\frac{d\langle i(t)\rangle_{Ts}}{dt} = \langle v_g(t)\rangle_{Ts} - d'(t)\langle v_{Cr}(t)\rangle_{Ts} \tag{9.a}$$

$$C\frac{d\langle v(t)\rangle_{Ts}}{dt} = d(t)\langle i_{Lr}(t)\rangle_{Ts} - \frac{\langle v(t)\rangle_{Ts}}{R} \tag{9.b}$$

As discussed before the inductor is flux balanced during the on-time interval only, so from putting the

Then:

$$\langle v_{Cr}(t)\rangle_{Ts} = \langle v(t)\rangle_{Ts} \tag{10}$$

Also it has been mentioned that resonant capacitor Cr receives energy from the inductor L during off-time interval and delivers energy to the load during the on-time interval, note that $C_r\int_0^{Ts} dv_{Cr}(t)dt = 0$, so from Fig. 5 considering energy balance in resonant capacitor

$$d(t)\langle i_{Lr}(t)\rangle_{Ts} = d'(t)\langle i_L(t)\rangle \tag{11}$$

Putting Eqs. (10) and (11) into Eq. (9)

$$L\frac{d\langle i(t)\rangle_{Ts}}{dt} = \langle v_g(t)\rangle_{Ts} - d'(t)\langle v(t)\rangle_{Ts} \tag{12.a}$$

$$C\frac{d\langle v(t)\rangle_{Ts}}{dt} = d'(t)\langle i_L(t)\rangle_{Ts} - \frac{\langle v(t)\rangle_{Ts}}{R} \tag{12.b}$$

Eq.12 indicates that despite the resonant circuit consisting of resonant capacitor Cr and resonant inductor Lr, and corresponding sinusoidal and co-sinusoidal time domain waveforms of resonant current and resonant capacitor voltage, the nonlinear averaged equation and so on dc conversion ratio does not depend on either one of them and their values or the switching period TS, but only depends on the operating duty ratio, D, as in conventional dc-dc converters.

4. Predictive Current Controller Design of the Hybrid-Switching Based Bridgeless PFC Converter

The proposed digital control algorithm [9] of the novel bridgeless PFC converter based on average current mode control is illustrated in Fig. 8. The predictive current control algorithm is derived based on the assumption that the bridgeless converter switching frequency is much higher than the line frequency so the input voltage, Vin, can be assumed as a constant in one switching cycle, Ts. In the outer voltage loop, the output voltage is sensed and compared with the voltage reference Vref. The error becomes the input of the voltage proportional-integral (PI) controller. The output of

this PI controller is the scaling factor for the rectified voltage that is used as one of the inputs to the multiplier. The product of the scaling factor and the rectified voltage divided by the square of the root mean square (RMS) of input voltage is the current reference, which is shown withi*ref in Fig. 8. The inner current loop implements average current mode control to force the average inductor current to follow the reference current.

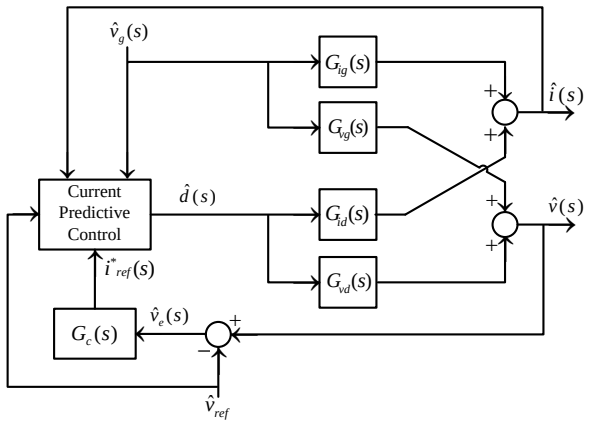

Fig. 8. Predictive Current Control (PCC) block diagram of the novel bridgeless PFC converter.

The averaged inductor current and capacitor voltage in one switching cycle of bridgeless boost converter are described in Eqs. (5) and (12). As discussed before this equations are the same for both negative and positive half cycle. Since the switching frequency is much higher than the line frequency,Eq. (9) can be expressed as:

$$i_L(t(n+1)) - i_L(t(n)) = \frac{V_g(t(n))T_s}{L} - \frac{(1-d(n))V_o(t(n))T_s}{L} \quad (13)$$

Where iL(t(n)), iL(t(n+1)) are the inductor current at the beginning of nth and (n+1)th switching cycles. The discrete time form ofEq. (13) for inductor current can be written as:

$$i_L(n+1) - i_L(n) = \frac{V_g(n)T_s}{L} - \frac{(1-d(n))V_o(n)T_s}{L} \quad (14)$$

This equation implies that the inductor current at the beginning of the next switching cycle is determined by the inductor current, the input voltage, the output voltage and the duty cycle at the present switching cycle. So the required duty cycle at the present switching cycle can be expressed as:

$$d(n) = \frac{L}{T_s}\frac{i_L(n+1) - i_L(n)}{V_o(n)} - \frac{V_o(n) - V_g(n)}{V_o(n)} \quad (15)$$

Now to force the inductor current to follow the reference current and control the output voltage to follow the reference voltage, iL(n+1) and Vo(n) are substituted by iref(n+1) and Vref(n) respectively. The desired duty cycle can be derived as:

$$d(n) = \frac{L}{T_s}\frac{i_{ref}(n+1) - i_L(n)}{V_{ref}(n)} - \frac{V_{ref}(n) - V_g(n)}{V_{ref}(n)} \quad (16)$$

Where

$$i_L(n+1) = V_{PI}.\left|\sin(\omega_{line}.t(n+1))\right| \quad (17)$$

In this equationVPI is the peak value of reference current, which is regulated by the output of the voltage loop regulator, as shown in Fig.8. Is the rectified line frequency sinusoidal waveform, which is stored as a look up table.In DSP implementation, the limitation value of the PI regulator is easily determined based on the rated load. The predictive algorithm in Eq. (16) can be use to generate the duty cycles and achieve near unity power factor in the implementation of PFC with novel bridgeless converter.

As shown in Fig. 8. The duty cycles are generated by the predictive algorithm. The rectified voltage Vinis sensed for peak value and zero cross signal detection. The peak value of the rectified voltage is used in the predictive algorithm implementation. The reference current, iref, is from the multiplier. Its amplitude is determined by the output of the PI controller in the voltage loop. Its phase and sinusoidal waveform are determined by the zero cross detection and the sine-wave look-up table. The output voltage Vo is controlled by the closed loop using a PI regulator. In this digital control system, the feedback signals are Voand Vin. The output is the gate signal for the switch. Consequently, no current loop is needed in the calculation of the duty cycle, all the duty cycles required to achieve unity power factor in a half line period can be generated in advance with this predictive current control strategy.

5. Simulation and Verification

Simulations have been carried out in the MATLAB/Simulink environment to verify the good performance of the proposed method. The following parameters as shown in Table 1 have been considered in the simulation.

Table 1. Simulation parameters

Key parameters	Values
Input voltage	110 VAC/ 50Hz
Output voltage	200 - 300VDC
Nominal Power	3kW
PWM carrier frequency	100kHz
L and C	1mH/ 10μF

The performances obtained with the novel bridgeless Boost converter using predictive current control are outlined in Figs. 9-12 operating at the desired output reference voltage Vref = 300V. The steady-state waveforms of the input voltage, current, and output voltage are shown in Fig. 9. The line THD is 2% and the power factor is 0.9997. The DC output voltage is stabilized at the reference value of 300 volts with a 1% ripple at 50 Hz. The output voltage stabilization for input voltage step change from 110V to 130V (RMS) have been illustrated in Fig. 10. The line current THD is 2.3% and the power factor is 0.993 with 3%overshoot in output voltage. Fig. 11 shows the output voltage stabilization for 50% load step change, which comes with 2.5% line current THD and the power factor of 0.9995 with 4% output voltage overshoot and 0.7 second response time. As shown in Fig. 12 the input current remained sinusoidal despite the

input voltage disturbance with the third harmonic (30% amplitude of fundamental harmonic).

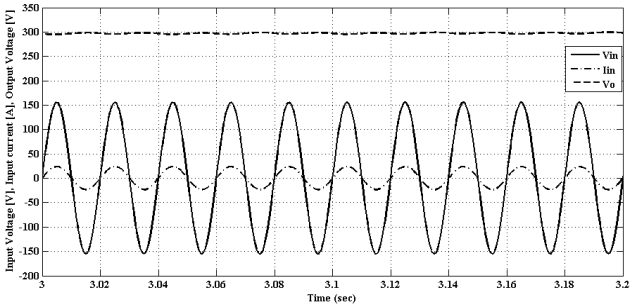

Fig.9. Input voltage, current and output voltage waveforms for full load.

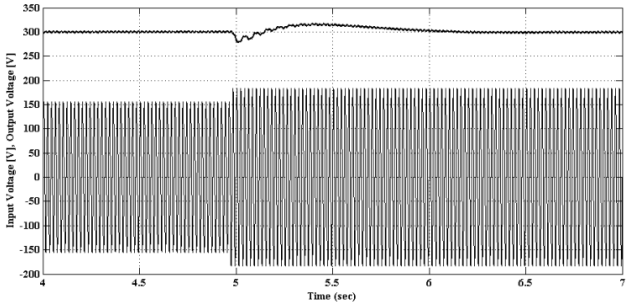

Fig.10. Output voltage stabilization for input voltage step change from 110V to 130V.

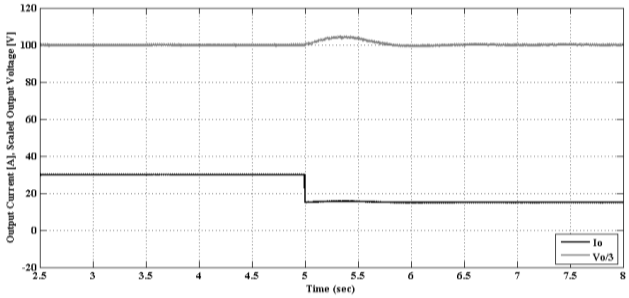

Fig.11. Output voltage stabilization for 50% load step change.

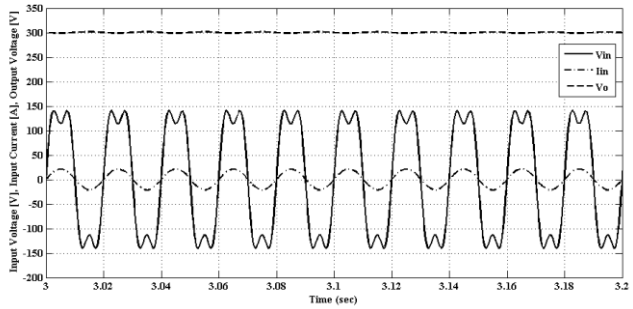

Fig.12. Input current and output voltage waveforms for disturbed input voltage.

As a case study the power factor and THD for bridgeless and conventional Boost rectifier are compared through the MATLAB simulation in Figs. 13-16. As illustrated in these figures using bridgeless Boost rectifier the power factor has been improved from 0.997 to more than 0.999 at similar load condition and THD has been improved from 4.5% to 2% compare to the conditional Boost based rectifier.

For more investigation the performance of both bridgeless and conventional Boost rectifiers between 1 per-unit to 2 per-units has been simulated through MATLAB. The outcome is summarized in two charts in Figs. 17-18. It can be concludedfrom these charts as output power increases from 1 pu to 2 pu the power factor decreases and total harmonic distortion increases for both bridgeless and conventional converters, which means both converters have their best performance on their full load condition. The most concerning subject in this investigation is that the bridgeless PFC rectifier shows better performance (higher power factor and lower THD) than the conventional one in all over power range from 1 pu to 2 pu.

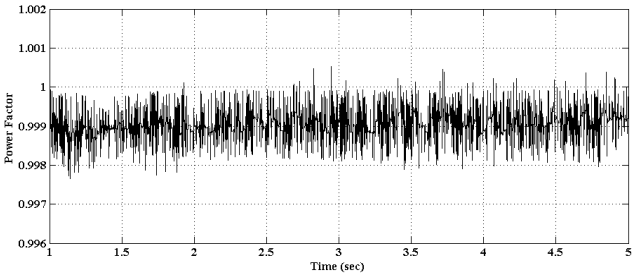

Fig.13. Power factor improvement of the bridgelessrectifier

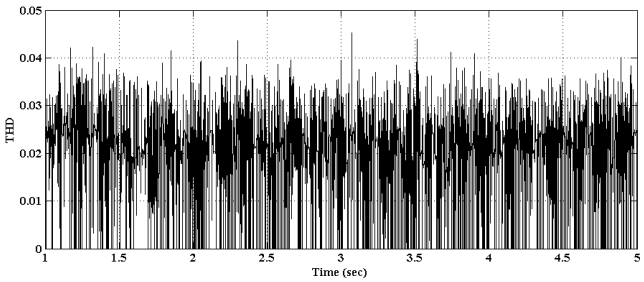

Fig.14. Input current total harmonic distortion of the bridgeless Boost rectifier

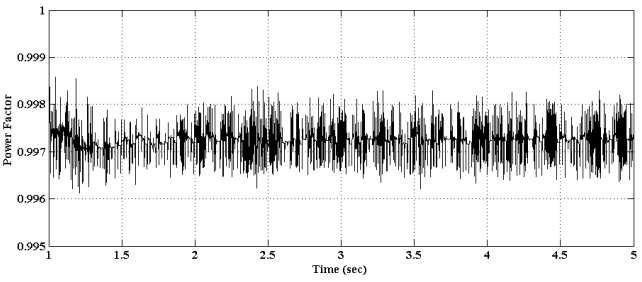

Fig.15. Power factor of conventional Boost based rectifier

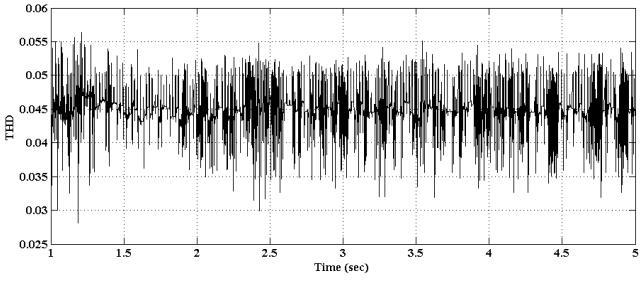

Fig.16. Input current total harmonic distortion of conventional Boost based rectifier

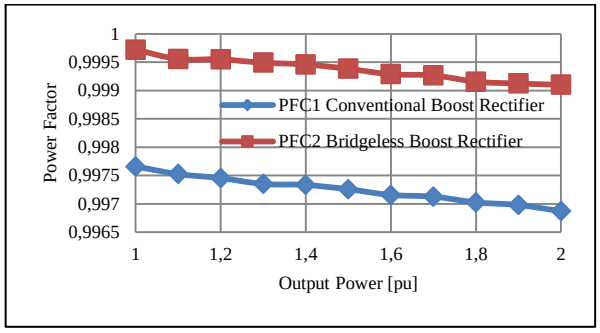

Fig.17. Power factor improvement of Bridgeless Boost rectifier compared to the conventional Boost rectifier

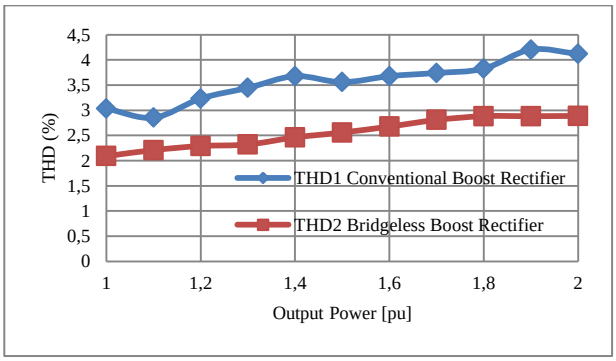

Fig.18. THD improvement of Bridgeless Boost rectifier compared to the conventional Boost rectifier

6. Conclusion

In this study, a hybrid switching based bridgeless PFC converter was investigated for on-board battery charger applications.Utilizing hybrid switching, which is the combination of square-wave PWM switching and resonant switching techniques, all full bridge rectifier elements were eliminated such that this converter operates directly from AC line.Eliminatingthe front-end full-bridge rectifierresulted in performance and size advantage over conventional bridge type PFC converters. To investigate the dynamic performance of this PFC circuit, the small-signal models were derived.The predictive current control algorithm was derived for this novel topology, consequently no current loop was needed in the calculation of the duty cycle, all the duty cycles required to achieve unity power factor in a half line period were generated in advance with predictive current control strategy.

Compared to the conventional Boost based PFC rectifier unity power factor and very low total harmonic distortion (THD) were achieved over wide input voltage and load current range using predictive current control. Tables II and III are supporting this assertion. Simulation results showed the effectiveness of using predictive current control for high efficient hybrid-switching based bridgeless PFC converter.

Table 2. Line current power factor comparison between conventional Boost and bridgeless Boost rectifier

P_o [pu]	1	1.2	1.4	1.6	1.8	2
Conventional Boost PF	0.9976	0.9974	0.9973	0.9971	0.9970	0.9968
Bridgeless Boost PF	0.9997	0.9995	0.9994	0.9992	0.9991	0.9991

Table 3. Line Current THD comparison between conventional Boost and bridgeless Boost rectifier

P_o [pu]	1	1.2	1.4	1.6	1.8	2
Conventional Boost THD	3.03	3.23	3.67	3.67	3.82	4.11
Bridgeless Boost THD	2.08	2.29	2.46	2.67	2.88	2.88

References

[1] J. Kim, G. Choe, H. Jung, B. Lee, Y. Cho, and K. Han. "Design and Implementation of a High-Efficiency On-Board Battery Charger for Electric Vehicles with Frequency Control Strategy" IEEEVehicle Power and Propulsion Conference, <http://ieeexplore.ieee.org/xpl/mostRecentIssue.jsp?punumber=5720573>pp. 1-6, September 2010.

[2] X. Yan, and D. Patterson "A High-Efficiency On-Board Battery Charger with Unity Input Power Factor" Australasian Universities Power Engineering Conference, pp.306-312, September 1999.

[3] M. Morcos, C. R. Mersman, G. G.Sugavanam, and N. G. Dillman, "Battery chargers for electric vehicles,"IEEE Power engineering Review, Vol. 20, No. 11, pp. 8-11, November 2000.

[4] Y. C. Chiang, Y. L. Ke, H. S. Chuang, and H. K. Chen, "Implementation and analysis of an improved series-loaded resonant dcdc converter operating above resonance for battery chargers,"IEEEIndustrial and Commercial Power Systems Technical Conference, pp. 1-8, May 2008.

[5] Y. C. Chuang and Y. L. Ke, "High-efficiency and low-stress ZVT-PWM DC-to-DC converter for battery charger,"IEEE Trans. Ind. Electron., Vol. 55, No. 8, pp. 3030-3037, August 2008.

[6] J. J. Chen, F. C. Yang, C. C. Lai, Y. S. Hwang, and R. G. Lee, "A high efficiency multimode Li-Ion battery charger with variable current source and controlling previous-stage supply voltage,"IEEE Trans. Ind. Electron., Vol. 56, No. 7, pp. 2469-2478, July 2009.

[7] S. Y. Tseng, T. C. Shin, S. Y. Fan, and G. K. Chang, "Design and implementation of lithium-ion/lithium-polymer battery charger with impedance compensation,"IEEE International Conference on Power Electronics and Drive Systems, pp. 866-870, November 2009.

[8] S. Cuk, "True Bridgeless PFC Converter Achieves Over 98% Efficiency, 0.999 Power Factor," Power Electronics Technology, Vol. 36, No. 8, pp. 34-40, August 2010.

[9] M.R. Abedi and F. Tahami, "Analysis and design of predictive control strategy for Sheppard-Taylor based PFC rectifier," 17th IEEE International Symposium on Industrial Electronics,pp. 397-402, July 2008.